IEEE Photonics Journal
An IEEE Photonics Society Publication

Ultraviolet-Extended Supercontinuum Generation in Zero-Dispersion Wavelength Decreasing Photonic Crystal Fibers

Volume 12, Number 6, December 2020

Wanjun Bi
Xia Li
Meisong Liao
Tianxing Wang
Peiwen Kuan
Liang Chen
Lili Hu
Weiqing Gao

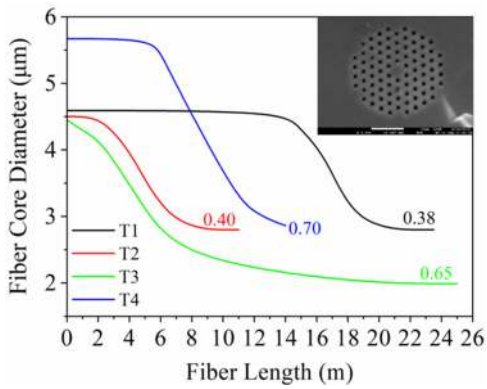

DOI: 10.1109/JPHOT.2020.3034235

Ultraviolet-Extended Supercontinuum Generation in Zero-Dispersion Wavelength Decreasing Photonic Crystal Fibers

Wanjun Bi,[1] Xia Li,[1] Meisong Liao,[1] Tianxing Wang,[1] Peiwen Kuan,[1] Liang Chen,[1,2] Lili Hu,[1] and Weiqing Gao[3]

[1]Key Laboratory of Materials for High Power Laser, Shanghai Institute of Optics and Fine Mechanics, Shanghai 201800, China
[2]University of Chinese Academy of Sciences, Beijing 10049, China
[3]School of Electronic Science and Applied Physics, Hefei University of Technology, Hefei 230009, China

DOI:10.1109/JPHOT.2020.3034235

Manuscript received August 16, 2020; revised October 19, 2020; accepted October 24, 2020. Date of publication October 27, 2020; date of current version November 6, 2020. This work was supported in part by the National Key Research and Development Program of China under Grant 2018YFB0504500, in part by the National Natural Science Foundation of China (NSFC) under Grants 61705244, 61307056, 61875052, and 61905258, in part by the Natural Science Foundation of Shanghai under Grants 17ZR1433900 and 17ZR1434200, and in part by the Chinese Academy of Sciences Pioneer Hundred Talents Program. Corresponding authors: Xia Li; Meisong Liao (e-mail: lixia.summerlee@gmail.com, liaomeisong@siom.ac.cn).

Abstract: Supercontinuum covering the ultraviolet-blue region is highly useful for fluorescence microscopy. Four zero-dispersion wavelength decreasing photonic crystal fibers with different fiber cross structures and taper profiles are fabricated to extend the short wavelength edge of supercontinuum. Both nanosecond and picosecond pump pulses at 1 μm are used to generate supercontinuum. With a 3 ns pump pulse, the short wavelength edge of supercontinuum is extended to below 400 nm in a fiber with high air-hole ratio (named T3). The underlying mechanism of supercontinuum generation is explored. The short and long wavelength edges of supercontinuum are highly related with the phase-matching condition which decided by the group velocity curve of fiber small core end. With a 10 ps pump pulse, the spectral intensity around ~800 nm increases in all four fibers. However, the intensity in shorter wavelength band decreased in fibers with a high air-hole ratio (named T3, T4). The experimental results imply that a zero-dispersion wavelength decreasing photonic crystal fiber suitable for nanosecond pulse pumping is not necessarily suitable for picosecond pulse pumping, especially for fibers with high air-hole ratio.

Index Terms: Supercontinuum generation, Photonic crystal fiber, nonlinear optics.

1. Introduction

Supercontinuum (SC), which covers broad spectral band, offers an attractive optical source in diverse applications like metrology [1], [2], biomedical imaging [3]–[5], and astronomy [6]. The SC in the ultraviolet-blue region is highly useful for fluorescence microscopy because many fluorescent molecules are excited in the wavelength range from ~600 to ~350 nm [7], [8]. Compared to conventional fiber, the chromatic dispersion and nonlinear properties of photonic crystal fiber (PCF) could be profoundly altered by modifying the PCF cross structure [9]–[11]. Therefore, the emergence of PCF brings a dramatic revolution to SC generation.

Due to the complexity of SC generation in general, the short wavelength edge of SC below 400 nm can be extended in more than one way, such as by using a PCF with a high air-hole ratio [12], by using a taper fiber [13]–[17], by using phase-matched higher-order fiber modes [18], and by using a short pump wavelength [14], [19], [20]. In 2008, SC spectrum extending from below 400 to 2450 nm was generated in a large-core high-air-hole ratio PCF pumped by a sub-ns pump source at 1064 nm [12]. In 2010, conversions into the spectral range of 300-470 nm at efficiencies as high as 40% were observed in tapered fiber when pumping at 523 nm [14]. The visible SC was obtained by fulfilling the phase-matching condition by coupling the pump into two guided modes of fiber [18]. Pumped by the second harmonic of 1 μm, SC spanning from 350 to 800 nm was obtained in a PCF taper with a core diameter of 0.92 μm [19].

Using a uniform PCF, the short wavelength edge of SC when pumped by commercially available lasers which operating at 1 μm is normally limited to approximately 450 nm [9]. The short wavelength edge of SC which determined by the group velocity profile can be shifted into blue by decreasing the core diameter or increasing the air-hole ratio of the uniform PCF. However, in this approach, the fiber zero-dispersion wavelength (ZDW) is away from the pump wavelength, and the intensity of the visible part of SC decreases. The ultraviolet-blue radiation with an enhanced intensity is hard to obtain in a simple uniform PCF [12].

The nonlinearity enhancement and dispersion engineering afforded by core size reduction in taper fiber allow for an additional degree of SC spectrum control, especially the short wavelength band. SC spanning from 370 to 1545 nm at the 20 dB level was generated in tapered standard telecommunication fiber with $\sim$2 μm diameter over a 90 mm length [13]. The generation of SC spectra was extended from the visible into the ultraviolet region in ZDW decreasing PCF when pumped by both nanosecond and picosecond sources at 1.064 μm [15]. SC with a very efficient power transfer from the pump to the visible region between 350 and 600 nm was obtained in a 10 m-long PCF with a 7 m-long section tapered down from 160 μm to 67 μm outer diameter [8]. An ultra-broad SC down to 280 nm in the deep UV was demonstrated by pumping sharply tapered (5-30 mm taper lengths) solid-core PCFs with 130 fs, and 2 nJ pulses at 800 nm [21]. In 2012, an ultraviolet-extended SC generation down to 352 nm was obtained in cascaded PCF tapers in a monolithic fiber when pumped at 1064 nm [16]. An ultra-broadband SC from 400 to 5140 nm was generated in a tapered ultra-high numerical aperture (NA) all-solid fluorotellurite fiber pumped by a 1560 nm mode-locked fiber laser [22]. Both the taper profile and the fiber cross structure (e.g., fiber core diameter, and air-hole ratio) could be changed to regulate the dispersion and nonlinearity characteristics of the taper fiber, hence, the SC generation process becomes more sophisticated, needs much more investigation.

In this study, four ZDW decreasing PCFs with different taper profiles and fiber cross structures are manufactured to investigate the SC generation process. The PCFs are drawn directly from fiber draw tower in our laboratory. An SC with a short wavelength edge lower than 400 nm is obtained when pumped by a laser with 3 ns pulse width and 1 μm wavelength. The underlying mechanism is explained combined with the ZDW position and the group-velocity curves. With 10 ps pump pulse width and 1 μm wavelength, the spectral intensity around $\sim$800 nm increases in all four fibers, however, the intensity in short wavelength band decreases in T3 and T4 with high air-hole ratio. The results imply that a ZDW decreasing PCF suitable for nanosecond pulse pumping is not necessarily suitable for picosecond pulse pumping. This systematical investigation could provide practical guidance to design PCF with decreasing ZDW.

2. Theory

SC generation process could be described by the generalized nonlinear Schrödinger equation:

$$\frac{\partial A}{\partial z} + \frac{\alpha}{2}A - \sum_{k\geq 2}\frac{i^{k+1}}{k!}\beta_k\frac{\partial^k A}{\partial t^k} = i\gamma(1-f_R)\left(|A|^2A - \frac{2i}{\omega_0}\frac{\partial}{\partial t}(|A|^2A)\right) + i\gamma f_R\left(1+\frac{i}{\omega_0}\frac{\partial}{\partial t}\right)\left(A\int_0^\infty h_R(t)\left|A(t-\tau)\right|^2 d\tau\right) \quad (1)$$

Table 1
Detailed Fiber Parameters of T1, T2, T3, and T4

	Air-hole diameter (μm)	Pitch (μm)	Air-hole diameter (μm)	Pitch (μm)
T1	1.10	2.91	0.72	1.89
T2	1.14	2.86	0.79	1.96
T3	2.21	3.38	1.15	1.76
T4	2.89	4.12	1.72	2.45

where, A is the envelope of the electric field in the retarded frame, z is the transmission distance, α is the fiber loss, β_k is the dispersion coefficients associated with the Taylor series expansion of the propagation constant $\beta(\omega)$ about the central angular frequency of the pump pulse ω_0, t is time, and γ is the nonlinear coefficient. The right-hand side of this equation mainly accounts for various nonlinear effects, such as self-phase modulation (SPM), Raman effect, and self-steeping effect.

The underlying mechanism for blue-shifting the SC spectra is as follows: first, the pump pulse in anomalous dispersion region is modulated by the modulation instability (MI) and evolves into a train of femtosecond soliton-like pulses with sufficient fiber length. The soliton pulses gradually red-shift under Raman effect while radiating dispersive waves (DWs) in the normal dispersion region. Initially, the group-velocities of DWs are smaller than those of soliton pulses and lag behind them. However, the soliton decelerates with its red-shifting and eventually temporally overlaps with DW. The soliton and DW then interact, leading to energy transfer to shorter wavelength band. The group-velocity of DW is decreased and lags behind soliton again. This process could repeat again and again as long as the soliton red-shifts. As a result, the DW is trapped by soliton and will not eventually disperse [7], [23], [24].

The interaction of soliton and DW generally dominates the short and long wavelength edges of SC. The phase-matching condition of soliton and DW could be described by the following equation:

$$\sum_{n\geq 2} \frac{(\omega_{DW} - \omega_S)^n}{n!} \beta_n(\omega_S) - (1 - f_R)\gamma P_S = 0 \tag{2}$$

where, ω_{DW} and ω_S are the frequencies of DW and soliton, respectively, f_R is the Raman fraction, and P_S is the peak power of soliton. The generated DW usually further extends into blue compared to that predicted by this phase-matching equation. This discrepancy would be caused by the spectral interaction through cross-phase modulation (XPM) and four-wave mixing process (FWM) [25], [26]. The phase matching of DW and soliton is strongly influenced by the group velocity variation [12].

3. Fiber Properties of Zero-dispersion Wavelength Decreasing Photonic Crystal Fibers

Four PCFs with different fiber cross structures and taper profiles were fabricated in our laboratory by the conventional stack-and-draw technique, which are referred to as T1, T2, T3, and T4, respectively. The four PCFs were made of pure silica material (index: approximately 1.45) with air-holes in the cladding (index: 1). The four PCFs had the same air-hole arrangement. Fig. 1(a) insert shows the scanning electron micrograph (SEM) of T1 cross section at the fiber large core end. The four PCFs were all single clad. The air-hole ratios for T1, T2, T3, and T4 were 0.38, 0.40, 0.65, and 0.7, respectively, which gradually increased. The fiber lengths for T1, T2, T3, and T4 were 23, 11, 25, and 14 m, respectively. Fig. 1(a) depicts the variation of fiber core diameter as a function of the fiber length. Table 1 presents the detailed fiber parameters. Fig. 1(b) illustrates the group velocity curves of fiber small core end of T1, T2, T3, and T4. Fig. 1(c) and (d) show the fiber dispersion of the fiber large and small core ends calculated using the finite element method. The following sectionpresents an investigation of SC generation based on the four PCFs.

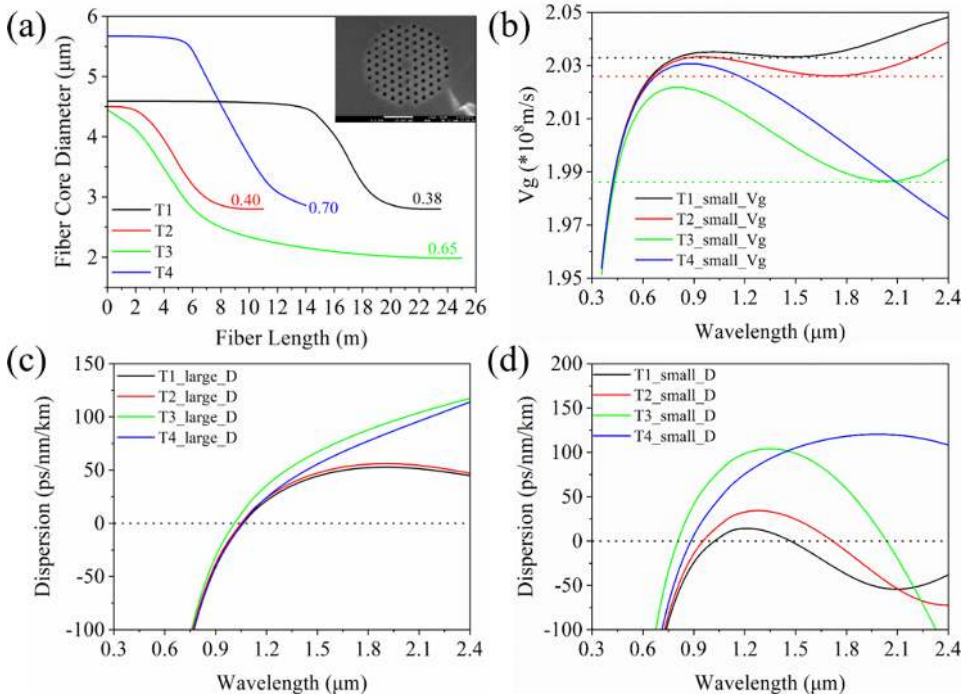

Fig. 1. (a) The fiber core diameter as a function of fiber length (The number marked in figure refers to the air-hole ratio of fiber). Insert: SEM of T1 cross section at the fiber large core end. (b) The group velocity of fiber small core end of T1, T2, T3, and T4. (c) The dispersion curve of the fiber large core end of T1, T2, T3, and T4. (d) The dispersion curve of the fiber small core end of T1, T2, T3, and T4.

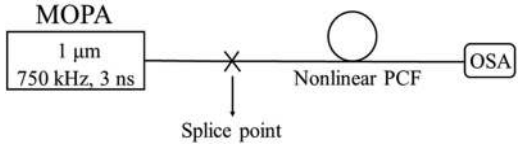

Fig. 2. The experimental setup with nanosecond pump pulse.

4. Supercontinuum Generation With Nanosecond Pump Pulse

Fig. 2 illustrates the experimental setup. The pump laser used for SC generation was a master oscillator power amplifier (MOPA) emitting 3 ns pulses at 1 μm wavelength and 750 kHz repetition rate. The nonlinear PCF was directly spliced to the MOPA pigtail. The output SC was measured by two optical spectrum analyzers with a wavelength ranging from 350 to 1700 nm and 1200 to 2400 nm.

For T1, the ZDW of fiber large core end was ~1066 nm. The fiber small core end had two ZDWs, ~1021 and ~1470 nm. Fig. 3(a) depicts the SC spectra in log scale. A peak with ~1600 nm center wavelength was generated in the long wavelength band, which was larger than the second ZDW of fiber small core end. The soliton cannot shift across the second ZDW of PCF, thus, the peak at ~1600 nm was determined to be a red shifted DW. Blue shifted DW was obtained at ~690 nm for SC output power of 1.06 W. With the increasing of pump power, a peak around 630 nm arose, ~60 nm further into the short wavelength band. The intensity of the ~630 nm peak also increased as the pump power increased. This may be caused by the sufficient interaction of soliton and DW through XPM effect due to the small group velocity variation of T1 (black line in Fig. 1(b)) [26]. This interaction also induced spectral ripples in the short wavelength band.

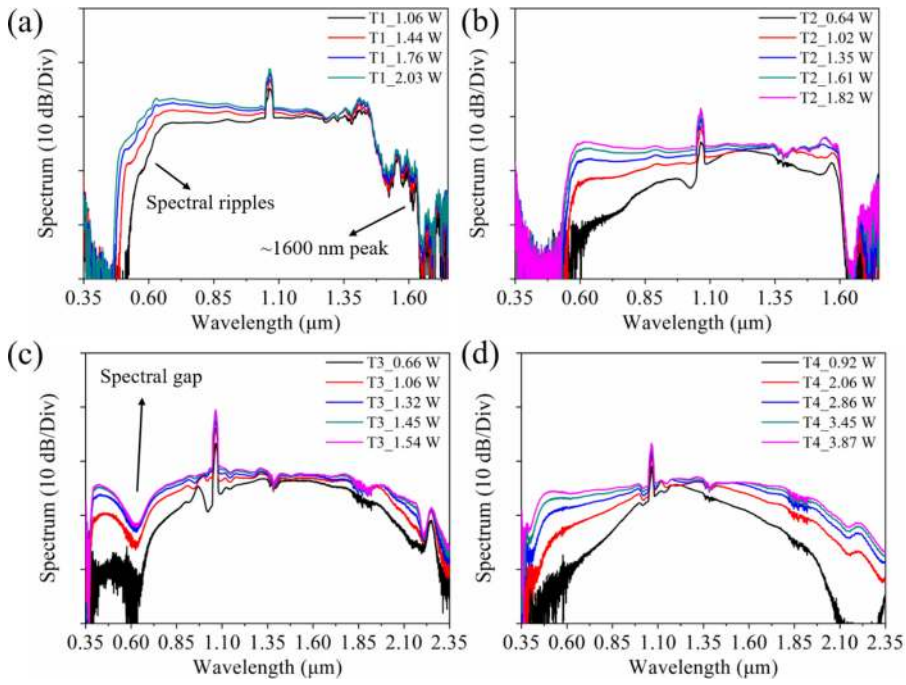

Fig. 3. SC generation with nanosecond pump pulse (the power shown in the legend is SC output power). (a) Measured SC spectra in T1. (b) Measured SC spectra in T2. (c) Measured SC spectra in T3. (d) Measured SC spectra in T4.

For T2, its air-hole ratio (0.40) was slightly larger than that of T1 (0.38). The ZDW of fiber large core end was ~1055 nm, the two ZDWs of the fiber small core end were ~950 and ~1719 nm. The long wavelength edge was approximately 1600 nm, and no red shifted DW was observed. The generated DW was at ~590 nm. The short wavelength edge was cleaner (no spectral ripples) compared to the SC spectra generated in T1 because the group velocity variation of T2 becomes large, and no obvious XPM effect occurred.

For T3, the air-hole ratio was larger (0.65). The ZDW of fiber large core end was ~1014 nm. The ZDWs of fiber small core end were ~803 and ~2038 nm. SC with short wavelength edge lower than 400 nm (approximately 380 nm) was obtained. The intensity of the short wavelength band was lower compared to that of the SC generated in T1. The fiber diameter at the distance of soliton fission determines the phase-matching condition for DW generation and thus the spectral position of DW. The 1 m fiber length was enough for soliton fission with 600 ps pump pulse width [15]. Thus, the soliton fission length for pump pulse with 3 ns pulse width in our experiment was several meters. However, there is no fiber section with constant diameter in the front of T3. That is, the fiber diameter, where soliton fission occurred, was small. The fiber ZDW was away from the pump pulse when soliton fission occurred. Generally, the proximity of the ZDW to the pump wavelength at the point of fission could result in a large spectral overlap with the DW and lead to substantial transfer of power on the blue side of the SC spectrum with a minor gap between the DW and pump spectral components. Thus, DW had a low intensity, and a spectral gap emerged between DW and other SC components in T3. From the group-velocity of the small fiber end in T2, the wavelength of the phase matched DW was much short due to its small fiber core diameter and large air-hole ratio. The short wavelength edge extended to 380 nm.

For T4, both the fiber core and air-hole ratio were larger to keep fiber ZDW of the fiber large core end around the pump wavelength. The ZDW of fiber large core end was ~1055 nm. An initial length of fiber with constant fiber core (~6 m) made the pump wavelength near fiber ZDW when soliton fission occurred. Thus, no spectral gap was observed in T4. Unfortunately, the diameter of fiber

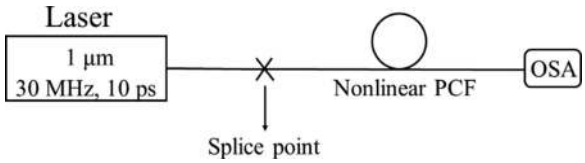

Fig. 4. The experimental setup with picosecond pump pulse.

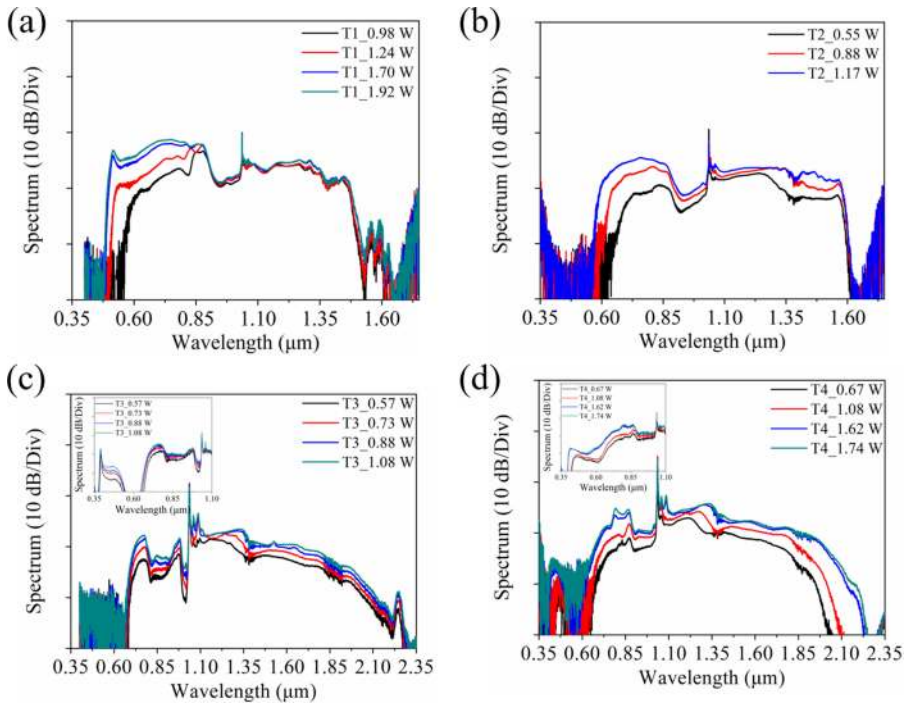

Fig. 5. SC generation with picosecond pump pulse (the power shown in the legend is SC output power). (a) Measured SC spectra in T1. (b) Measured SC spectra in T2. (c) Measured SC spectra in T3. (d) Measured SC spectra in T4.

small core end was large. The fiber nonlinearity was not high enough to enable sufficient soliton shift as far as that in T3. Eventually, SC spanning from 400 to 2350 nm was obtained.

5. Supercontinuum Generation With Picosecond Pump Pulse

Fig. 4 shows the experimental setup for picosecond pump pulse. The pump laser used for the SC generation was a mode-locked fiber laser emitting 10 ps pulses at 1 μm wavelength and 30 MHz repetition rate. The nonlinear PCF was also directly spliced to the fiber laser pigtail.

Compared with nanosecond pumping, the SC spectra with picosecond pumping are interesting. The spectral intensity around ~800 nm became larger for all four fibers. For T1 and T2 with low air-hole ratio, the spectral width was almost the same with that in nanosecond pulse pumping. For T3 and T4 with high air-hole ratio, the spectral intensity at shorter wavelength (below 600 nm) became weaker. When SC spectra were measured, a sphere was used to collect SC spectra into the optical spectral analyzer. The sphere had a great average attenuation (in the order of 10^{-5}) of SC. When the pulse width of pump was 10 ps, SC at short wavelength band was almost undetectable in T3, while that in T4 had a small peak only. The short wavelength band of SC was measured with a multimode fiber to collect SC (insert, Figs. 5(c) and (d)). We suspected that this phenomenon occurs because DW around ~800 nm was directly generated by the initially formed soliton. Soliton with higher peak

power and shorter pulse width was formed when picosecond pump pulse was used. The DW at shorter wavelength band (below 600 nm) was indirectly generated through the interaction between DW and soliton (e.g., FWM and XPM effects). With soliton redshifts, the energy radiated by the soliton at the long wavelength to short wavelength exponential decay with increased frequency detuning [23]. For picosecond pump pulse, the soliton order was much less (in the order of 10^{-3}) than that with nanosecond pump pulse. Thus, the spectral intensity below 600 nm shrunk. For T1 and T2 with low air-hole ratio, the group-velocity was flat. As a result, the interaction between DW and soliton repeated for much more times compared to that in T3 and T4 with high air-hole ratio. The spectral intensity below 600 nm was not significantly reduced, implying that a tapered fiber suitable for nanosecond pulse pumping is not necessarily suitable for picosecond pulse pumping. Note that the repetition rate of the nanosecond pump pulse was quite different from that of the picosecond pump laser. However, SC spectral was mainly decided by the pulse width and the peak power of the pump pulse. The repetition rate increase could only scale the SC output power.

6. Conclusion

In summary, four PCFs with decreasing ZDW were directly fabricated from fiber draw tower in our laboratory. These PCFs had different fiber cross structures and taper profiles. Both nanosecond and picosecond pump pulses at 1 μm were used for SC generation. With 3 ns pump pulse, the short wavelength edge of SC extended to 400 nm in T3 and T4. The short and long wavelength edges of SC were highly related with the phase-matching condition decided by the group velocity curve of fiber small core end. The fiber ZDW at the point when soliton fission occurred determined the phase-matching condition for DW generation and thus the DW spectral position. With 10 ps pump pulse, the spectral intensity around $\sim$800 nm increased in all four fibers, but the intensity in short wavelength band decreased in T3 and T4 with high air-hole ratio, implying that a ZDW decreasing PCF suitable for nanosecond pulse pumping is not necessarily suitable for picosecond pulse pumping, especially for fibers with large air-hole ratio. This investigation provides practical guidance to designing PCF with decreasing ZDW: (1) ZDW decreasing PCF with high air-hole ratio is more suitable for nanosecond pump pulse. (2) The ZDW when soliton fission occurs is of vital importance, determining the position of initial DW and SC flatness.

References

[1] H. N. Paulsen, K. M. Hilligsoe, J. Thogersen, S. R. Keiding, and J. J. Larsen, "Coherent anti-stokes raman scattering microscopy with a photonic crystal fiber based light source," *Opt. Lett.*, vol. 28, no. 13, pp. 1123–1125, Jul. 2003.
[2] C. Chen, W. Shi, R. Reyes, and V. X. D. Yang, "Buffer-averaging super-continuum source based spectral domain optical coherence tomography for high speed imaging," *Biomed. Opt. Express*, vol. 9, no. 12, pp. 6529–6544, Dec. 2018.
[3] M. K. Lu, H. Y. Lin, C. C. Hsieh, and F. J. Kao, "Supercontinuum as a light source for miniaturized endoscopes," *Biomed. Opt. Express*, vol. 7, no. 9, pp. 3335–3343, Sep. 2016.
[4] J.-P. Syu, W. Buddhakosai, S.-J. Chen, C.-C. Ke, S.-H. Chiou, and W.-C. Kuo, "Supercontinuum source-based multi-contrast optical coherence tomography for rat retina imaging," *Biomed. Opt. Express*, vol. 9, no. 12, pp. 6132–6144, Dec. 2018.
[5] J. Cascante-Vindas, F. Siles Canales, A. Diez Cremades, and M. V. Andres Bou, "Novel spectra in the supercontinuum generation with applications in the biodiversity conservation," in *Proc. Int. Work Conf. Bio-Inspired Intell.*, pp. 76–81, 2014.
[6] A. Ravi *et al.*, "Visible-Spanning flat supercontinuum for astronomical applications," *J. Lightw. Technol.*, vol. 36, no. 22, pp. 5309–5315, Nov. 2018.
[7] M. H. Frosz, P. M. Moselund, P. D. Rasmussen, C. L. Thomsen, and O. Bang, "Increasing the blue-shift of a supercontinuum by modifying the fiber glass composition," *Opt. Express*, vol. 16, no. 25, pp. 21076–21086, Dec. 2008.
[8] A. Kudlinski, M. Lelek, B. Barviau, L. Audry, and A. Mussot, "Efficient blue conversion from a 1064 nm microchip laser in long photonic crystal fiber tapers for fluorescence microscopy," *Opt. Express*, vol. 18, no. 16, pp. 16640–16645, Aug. 2010.
[9] J. M. Dudley, G. Genty, and S. Coen, "Supercontinuum generation in photonic crystal fiber," *Rev. Mod. Phys.*, vol. 78, no. 4, pp. 1135–1184, Oct. 2006.
[10] C. Huang *et al.*, "Ultraflat, broadband, and highly coherent supercontinuum generation in all-solid microstructured optical fibers with all-normal dispersion," *Photon. Res*, vol. 6, no. 6, pp. 601–608, Jun. 2018.
[11] H. Yang *et al.*, "Impact of the self-steepening effect on soliton spectral tunneling in PCF with three zero dispersion wavelengths," *Chin. Opt. Lett.*, vol. 16, no. 7, 2018, Art. no. 070601.

[12] J. M. Stone and J. C. Knight, "Visibly "white" light generation in uniform photonic crystal fiber using a microchip laser," *Opt. Express*, vol. 16, no. 4, pp. 2670–2675, Feb. 2008.
[13] T. A. Birks, W. J. Wadsworth, and P. S. Russell, "Supercontinuum generation in tapered fibers," *Opt. Lett.*, vol. 25, no. 19, pp. 1415–1417, Oct. 2000.
[14] S. P. Stark, A. Podlipensky, N. Y. Joly, and P. S. J. Russell, "Ultraviolet-enhanced supercontinuum generation in tapered photonic crystal fiber," *J. Opt. Soc. Am. B*, vol. 27, no. 3, pp. 592–598, Mar. 2010.
[15] A. Kudlinski *et al.*, "Zero-dispersion wavelength decreasing photonic crystal fibers for ultraviolet-extended supercontinuum generation," *Opt. Express*, vol. 14, no. 12, pp. 5715–5722, Jun. 2006.
[16] H. H. Chen, Z. L. Chen, X. F. Zhou, and J. Hou, "Ultraviolet-extended flat supercontinuum generation in cascaded photonic crystal fiber tapers," *Laser Phys. Lett.*, vol. 10, no. 8, 2013, Art. no. 085401.
[17] H. H. Chen, Z. L. Chen, X. F. Zhou, and J. Hou, "Cascaded PCF tapers for flat broadband supercontinuum generation," *Chin. Opt. Lett.*, vol. 10, no. 12, 2012, Art. no. 120603.
[18] C. Lesvigne *et al.*, "Visible supercontinuum generation controlled by intermodal four-wave mixing in microstructured fiber," *Opt. Lett.*, vol. 32, no. 15, pp. 2173–2175, Aug. 2007.
[19] J. Cascante-Vindas *et al.*, "Tapering photonic crystal fibres for supercontinuum generation with nanosecond pulses at 532 nm," *Opt. Commun.*, vol. 281, no. 3, pp. 433–438, Sep. 2008.
[20] C. Li *et al.*, "Octave-spanning visible supercontinuum generation from an aluminum nitride single crystal pumped by a 355 nm nanosecond pulse," *Chin. Opt. Lett.*, vol. 16, no. 4, 2018, Art. no. 043201.
[21] S. Stark, J. Travers, and P. S. J. Russell, "Extreme supercontinuum generation to the deep uV," *Opt. Lett.*, vol. 37, no. 5, pp. 770–772, Mar. 2012.
[22] Z. X. Jia *et al.*, "Supercontinuum generation covering the entire 0.4-5 mu m transmission window in a tapered ultra-high numerical aperture all-solid fluorotellurite fiber," *Laser Phys. Lett.*, vol. 15, no. 2, Jan. 2018.
[23] J. M. Dudley and J. R. Taylor, *Supercontinuum Generation in Optical Fibers*. New York, NY, USA: Cambridge Univ. Press, 2010.
[24] A. V. Gorbach and D. V. Skryabin, "Light trapping in gravity-like potentials and expansion of supercontinuum spectra in photonic-crystal fibres," *Nat. Photon.*, vol. 1, no. 11, pp. 653–657, Nov. 2007.
[25] N. Wang, J.-H. Cai, X. Qi, S.-P. Chen, L.-J. Yang, and J. Hou, "Ultraviolet-enhanced supercontinuum generation with a mode-locked Yb-doped fiber laser operating in dissipative-soliton-resonance region," *Opt. Express*, vol. 26, no. 2, pp. 1689–1696, Jan. 2018.
[26] G. Genty, M. Lehtonen, and H. Ludvigsen, "Effect of cross-phase modulation on supercontinuum generated in microstructured fibers with sub-30 fs pulses," *Opt. Express*, vol. 12, no. 19, pp. 4614–4624, Sep. 2004.